Microfluidics and Nanofluidics (2019) 23:3
https://doi.org/10.1007/s10404-018-2159-9

RESEARCH PAPER

Hydrodynamics maneuver of a single helical flagellum swimming robot at low-Reynolds condition

Hassan Sayyaadi[1] · **Shahnaz Bahmanyar**[1]

Received: 30 March 2018 / Accepted: 8 November 2018 / Published online: 3 December 2018

Abstract

Helical swimming robots with a capable propulsion system at low-Reynolds numbers have been proposed for many applications. Although linear propulsion characteristics of swimming robots with a single helical flagellum have been extensively studied, the characteristics of maneuverability have not been completely investigated yet. This study presents a new method for the maneuverability of the helical swimming robot with a single helical flagellum. This mechanism is based on the change in the angle between the helical and body axes. This study shows that a change in the aforementioned angle can enable the swimming robot to have turning maneuvers in clockwise or counterclockwise directions. Moreover, the swimming robot will move in a straight line if the helical and body axes are parallel. To investigate this new method and predict the robot's behavior at various inclination angles, a hydrodynamics model is used. To validate the hydrodynamics model, an experimental prototype of a macro-size swimming robot with specific inclination angles is fabricated. The results indicate that the helical swimming robot swims on circular trajectories through specific inclination angles between the helical flagellum and the body axis. Moreover, the radius of curvature decreases by increasing the inclination angle. Results of the validated hydrodynamics model indicate that the turning velocity has approximately a constant value at different inclination angles depending on the rotational frequency and geometrical parameters of the swimming robot. Finally, the effects of geometrical parameters of the body and the helical flagellum on the radius of curvature and turning velocity are investigated through the proposed hydrodynamics model. The verified results indicate that the hydrodynamics model provides a viable alternative model to predict the behavior of a helical swimming robot at various inclination angles within a range of design variables. This new method can be introduced as a mechanism for maneuverability of the helical swimming robots with a single helical flagellum and will be able to control the parameters in this type of swimmers for the implementation of predefined missions.

Keywords Helical swimmer robot · Single helical flagellum · Hydrodynamics maneuver · Flagellum inclination angle

Abbreviations

d_{body}	Cylindrical body diameter (mm)
L_{body}	Cylindrical body length (mm)
$2b$	Helical tail diameter (mm)
$2h_{\text{helix}}$	Helical wave amplitude (mm)
L_{tail}	Helical tail's length (mm)
L_{total}	Overall length of swimmer robot (body length + helical tail) (mm)
β	Pitch angle (°)
α	Inclination angle (°)
λ	Helical wave length (mm)
n	Number of wavelengths (−)
W	Total weight (g)
D_{motor}	DC-motor diameter (mm)
L_{motor}	DC-motor length (mm)
V_{motor}	Voltage of motor (V)
$\text{vol}_{\text{battery}}$	Volume of battery (m^3)
V_{battery}	Voltage of battery (V)
ρ	Density of test fluid (Kg/m^3)
v	Kinematic viscosity (cSt)
f	Spinal propulsive frequency (Hz)
G	The center of mass $G = (x_g, y_g, z_g)$ (mm)
B	The center of buoyancy $B = (x_B, y_B, z_B)$ (mm)
$\vec{F}_{\text{helix}}$	Propulsive force in x-direction

✉ Hassan Sayyaadi
sayyaadi@sharif.edu

Shahnaz Bahmanyar
bahmanyar@mech.sharif.edu

[1] Department of Mechanical Engineering, Center of Excellence in Hydrodynamics and Dynamics of Marine Vehicles, Sharif University of Technology, Tehran, Iran

$\vec{M}_{\text{helix}}$	Torque resulting from fluid reaction on the helical tail
$\vec{F}_{\text{body}}, \vec{M}_{\text{body}}$	Viscous drag and torque acting on the body
$\vec{F}_{\text{e}}, \vec{M}_{\text{e}}$	External forces and torques that affect the swimmer
df_n, df_t	Hydrodynamic forces acting on a cylindrical element of local length
ξ_n, ξ_t	Local drag coefficient for motion normal and tangential to local length
υ_n, υ_t	Components of local normal and tangential to local length (mm/s)
G_{body}	The resistive matrix for the body
G_{helix}	The resistive matrix for the helical flagella
Ω	Angular velocity of the swimmer robot in inertial coordinates $\Omega = (\dot{\theta}, \dot{\phi}, \dot{\Psi})$ (rad/s)
R	Radius of curvature (mm)
U	Planer velocity of swimmer robot (mm/s)
v	Velocity of the swimmer robot in body-fixed coordinates $v = (v_x, v_y, v_z)$ (mm/s)
V	Velocity of the swimmer robot in inertial coordinates $V = (V_x, V_y, V_z)$ (mm/s)
Ω	Angular velocity of the swimmer robot in body-fixed coordinates $\Omega = (\Omega_x, \Omega_y, \Omega_z)$ (rad/s)

1 Introduction

Swimming robots are effective devices for various medical and industrial applications with predefined missions based on their micro- or macro-scale dimensions, since their motion is inspired by mechanisms of locomotion in microorganisms. Medical applications, such as delivering targeted drug, destroying blood clots in arteries, and imaging damaged areas, are some examples to which micro-sized swimming robots can be applied (Edd et al. 2003; Nelson et al. 2010; Feng and Cho 2014). As an industrial application, macro-scale swimmers can inspect and image the pipes that carry highly viscous fluids. Therefore, in view of different applications considered for such swimming robots, it is essential to investigate their maneuverability, controllability, and movability in different directions. In this respect, in low-Reynolds number conditions, microorganisms with helical flagellums are considered efficient swimmers with regard to their propulsion forces (Purcell 1997). Inspired by this fact, researchers have attempted to carry out extensive research studies on these swimmers and, then, design and fabricate them for several applications. In the studies with internal actuation, the linear propulsion characteristic (the straight locomotion as in movement in a straight line) of helical swimming robots with a single flagellum was analyzed experimentally in an unbound fluid condition (Behkam and Sitti 2006; Xu et al. 2015) or inside circular channels (Tabak and Yesilyurt 2013; Temel and Yesilyurt 2013).

Brennen and Winet (1977), Johnson and Brokaw (1979), Pak and Lauga (2014), and Elgeti et al. (2015) presented a review of propulsion parameters of microorganisms with theoretical models. In addition, Keller and Rubinow (1976) investigated the geometrical properties and swimming trajectories for swimming robots using the aforesaid hydrodynamic models.

For more than 50 years, hydrodynamics modeling of prokaryote microorganisms with helical tails has received much attention. In this regard, Gray and Hancock in 1955 put forward well-known theories of the resistive force theory (RFT) and slender body theory (SBT). Subsequently, Lighthill and Lighthill (1975) improved the SBT theory by considering the flow around the helical tail and the body–fluid interaction.

Other studies (e.g., studies of Nourmohammadi et al. 2016; Chen et al. 2010) on maneuvering of the helical swimmer considered multiple flagella actuated by several motors and introduced more rotating tails with various angular velocities generated by three-dimensional maneuverability. One of the major disadvantages of using several flagella is an increase in the size of the body and the degradation of motors.

In this paper, a new method is used that enables a single helical robot to have clockwise or counterclockwise maneuvers.

To the best of the authors' knowledge, there are no theoretical and experimental studies which have investigated and used this method, which can perform reorientation maneuvers on a single helical swimming robot with an internal actuation during swimming.

This study intends to clarify that the helical swimming robot can maneuver in a clockwise or counterclockwise direction through an inclination angle between body axis and helical flagellum. In addition, this study will show how this angle could affect the rotational velocity and trajectory. This paper is organized as follows. In Sect. 2, geometric and kinematic models of the swimmer and related equations of motion are presented; then, a hydrodynamics model based on RFT method is used to predict trajectories of the swimmer at various simulated inclination angles. In Sect. 3, an experimental prototype of a macro-scale swimming robot with specific inclination angles is fabricated to verify the hydrodynamics model. Then, experimental data are compared to the results of the proposed model. In Sect. 4, the behavior of the swimming robot at different inclination angles is predicted using the proposed hydrodynamics model. Moreover, the relationship of the inclination angles with the radius of curvature and rotational and angular velocities is illustrated. Finally, the effects of geometrical parameters of the body

and helical flagellum on the maneuverability characteristics are investigated.

2 Hydrodynamics modeling of a single-flagellum swimming robot

2.1 Definition

In this study, a swimming robot is designed and fabricated, which is inspired by the structure of prokaryote microorganism with a monotrichous flagellation. This robot is composed of two main sections: an elliptical body and a helical flagellum, whose geometry can be observed in Fig. 1. In this figure, (D_{body}) is the diameter, and (L_{body}) is the length of an elliptical body, which is connected to a helical flagellum by coupling. $(2h_{\text{helix}})$, (β), $(2b)$, and(λ) are the helical wave amplitude, the helix pitch angle, the diameter of helix cross section, and wavelength, respectively, with the wavelength number (n). The swimmer is propelled forward as the helical flagellum spins at angular velocity ofω in a counterclockwise direction around its main axis.

The inertial coordinate frame is denoted by (X, Y, Z) and the body-fixed coordinate frame by (e_x, e_y, e_z), which are attached to the mass center of the swimmer's body. To investigate the proposed method, the angle between the axis of the helical flagellum and the swimmer's body axis (e_x) is defined as the inclination angle (α), which is in the range of $\{0 \le \alpha < 90\}$ (Fig. 2).

In this paper, it is assumed that the helical propulsion system is composed of a single helical flagellum and an internal actuation system. When the axis of the helical flagellum is aligned with its body axis, the center of mass $\text{CG} = (x_g, y_g, z_g)$ is parallel to the center of buoyancy $B = (x_B, y_B, z_B)$. When the axis of a helical flagellum is inclined towards its body axis, the variation of the mass center becomes small enough to ignore. Therefore, the translation and orientation of the swimming robot can be defined according to the center of mass position $(\text{CG} = (x_g, y_g, z_g))$. A helical swimming robot swims with linear velocity of $v = (v_x, v_y, v_z)$ and angular velocity of $\Omega = (\Omega_x, \Omega_y, \Omega_z)$,

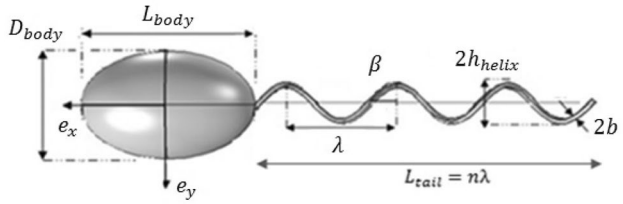

Fig. 1 Geometric parameters of the helical swimming robot in the body reference frame

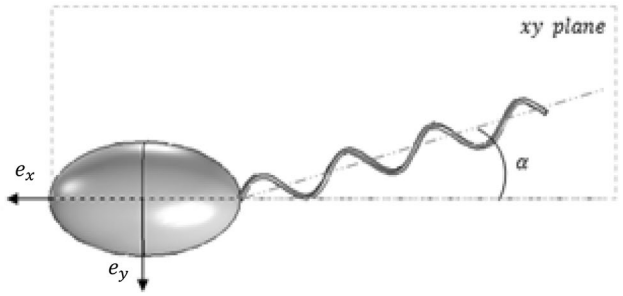

Fig. 2 Schematic illustration of the angleα as the angle between the helical flagellum and the body axis in the analytical range of $\{0 \le \alpha < 90\}$

caused by the rotation of the helical flagellum in the body-fixed coordinate (Fig. 3).

2.2 Dynamics modeling

The governing equations of motion are used to investigate the forces and torques exerted on the body of the swimming robot when the inclination angle is considered. To simplify the calculations and eliminate wall effects, a proper distance between the swimmer and tank walls is considered during swimming. Other assumptions considered in these computations include the slenderness of the helical flagellum ($b \ll L_{\text{tail}}$) and the ellipsoidal shape of the body of the swimming robot, which are different from the physical robot used in the experimentations. Figure 4 shows the directions of the torques and forces generated by the inclination angle between the helical flagellum and body axis.

When the helical flagellum axis is aligned with the swimmer's body axis, the thrust force generated by the helical flagellum is in parallel with the body axis, and the swimmer moves in a straight path. However, when the axis of the helical flagellum is not collinear with the symmetry axis of the body, the inclination angle is implemented, and the swimmer rotates in a specific direction, which will be discussed later.

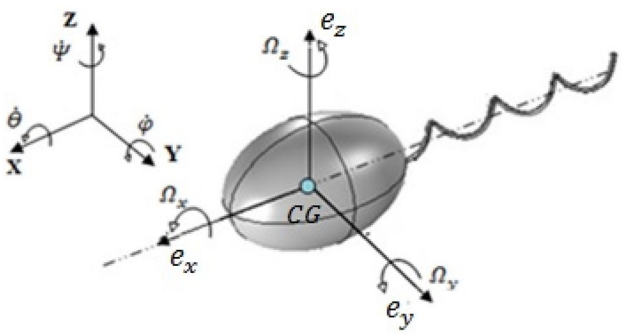

Fig. 3 Schematic model of the helical swimmer robot with its selective frames

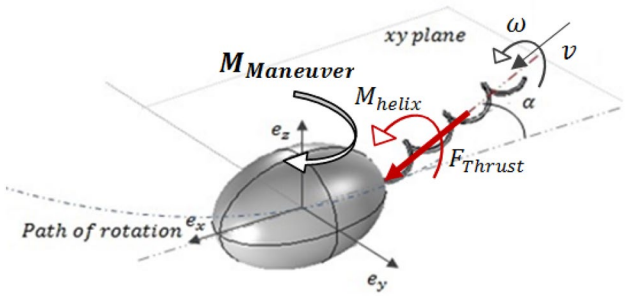

Fig. 4 Schematic model of swimmer robot and the direction of the forward and angular velocities depend on the inclination angle between the helical flagellum and body axis

Due to the inclination angle between the helical flagellum and the body axis, two components of thrust force are produced in e_x and e_y directions. Therefore, components of the thrust force produce a torque on the body whose rotation axis is perpendicular to the axis of the helical swimmer's trajectory. Considering the condition of low-Reynolds numbers and lack of acceleration, the governing equations of motion can be defined by considering the inclination angle in the force free–torque free manner as follows:

$$\vec{F}_{\text{Thrust}} - \vec{F}_{\text{body}} = \vec{F}_{\text{e}}, \tag{1}$$

$$\vec{F}_{\text{Thrust}} \times \overrightarrow{PG} + \vec{M}_{\text{helix}} - \vec{M}_{\text{body}} = \vec{M}_{\text{e}}. \tag{2}$$

In the above equations, $\vec{F}_{\text{Thrust}} = (F_x^{\text{Thrust}}, F_y^{\text{Thrust}}, 0)$ and $\vec{M}_{\text{helix}} = (M_x^{\text{helix}}, M_y^{\text{helix}}, 0)$ consist of the overall viscous forces and torques acting along the helical flagellum on xy plane; $\overrightarrow{\text{PG}} = (\text{PG}_x, \text{PG}_y, \text{PG}_z)$is the distance from the positions of acting forces and torques to the mass center of the helical swimming robot.

$\vec{F}_{\text{body}} = \left(F_x^{\text{body}}, F_y^{\text{body}}, 0\right)$ and $\vec{M}_{\text{body}} = \left(M_x^{\text{body}}, M_y^{\text{body}}, M_z^{\text{body}}\right)$ denote the viscous drag and torque acting on the swimmer's body, respectively. $\overrightarrow{F_{\text{e}}}$ and $\overrightarrow{M_{\text{e}}}$ are the external forces and torques that affect the swimmer in different directions, which are equal to zero, since the swimming robot is a free swimmer. To calculate the distribution of forces and torques on the moving helix, according to the resistive force theory, it can be assumed that the hydrodynamic forces acting on the slender helix moving through the fluid per a small filament of length ds are locally proportional to relative velocity V (Gray and Hancock 1955). These drag forces are considered as a tangential force component and a normal force component, respectively.

$$\text{d}f_n = -\xi_n v_n \text{d}s, \quad \text{d}f_t = -\xi_t v_t \text{d}s, \tag{3}$$

where ξ_n and ξ_t are the corresponding viscous drag coefficients; v_n and v_t are considered as the normal and tangential velocity components on an infinitesimally small filament of length ds (Gray and Hancock 1955; Chawng and Wu 1971):

$$\begin{bmatrix} \text{d}F_x^{\text{helix}} \\ \text{d}F_y^{\text{helix}} \end{bmatrix} = \begin{bmatrix} \cos(\beta) & -\sin(\beta) \\ \sin(\beta) & \cos(\beta) \end{bmatrix} \begin{bmatrix} df_n \\ df_t \end{bmatrix}. \tag{4}$$

In the above equation, $\text{d}F_x^{\text{helix}}$ and $\text{d}F_y^{\text{helix}}$ denote the tangential and normal viscous forces along the helical flagellum axis, respectively. The components of tangential and normal forces along the helical flagellum axis are derived, and the thrust force and required torque on a flagellum can be written, as shown in Eq. (5):

$$\vec{F}_{\text{helix}} = \int_0^{n\lambda} \overrightarrow{\text{d}F}_{\text{helix}}, \quad \vec{M}_{\text{helix}} = \int_0^{n\lambda} \overrightarrow{\text{d}M}_{\text{helix}}. \tag{5}$$

A very important property of the linearity of the Stokes flow is the linear relationship among body's velocity v, angular velocity Ω, external force F, and external torque M; these are in a linear relationship with each other and can be represented by a matrix equation of the following matrix format (Purcell 1997):

$$\begin{bmatrix} F \\ M \end{bmatrix} = [G]_{5\times5} \begin{bmatrix} v \\ \Omega \end{bmatrix}_{5\times1}, \tag{6}$$

where $[G]$denotes the viscous resistance matrix with the hydrodynamic parameters of the helical flagellum and body, represented by $H_{ij}^{\in\gamma}$ and $B_{ij}^{\in\gamma}$, respectively. For superscript $\in\gamma$, $\in$denotes the force or torque, and γ represents the velocity or angular velocity achieved by an acting force or a torque; i indicates the direction corresponding to $\in$, and j indicates the direction corresponding to γ.

The above-mentioned principles and hydrodynamics model for the helical swimmer were used. According to the physical locomotion of the maneuverable swimming robot, the resistance matrix of the elliptical body can be written as follows:

$$\begin{bmatrix} F_x^{\text{body}} \\ F_y^{\text{body}} \\ M_x^{\text{body}} \\ M_y^{\text{body}} \\ M_z^{\text{body}} \end{bmatrix} = \overbrace{\begin{bmatrix} B_{xx}^{FU} & 0 & 0 & 0 & 0 \\ 0 & B_{yy}^{FU} & 0 & 0 & 0 \\ 0 & 0 & B_{xx}^{M\Omega} & 0 & 0 \\ 0 & 0 & 0 & B_{yy}^{M\Omega} & 0 \\ 0 & 0 & 0 & 0 & B_{zz}^{M\Omega} \end{bmatrix}}^{G_{\text{body}}} \begin{bmatrix} v_x \\ v_y \\ \Omega_x \\ \Omega_y \\ \Omega_z \end{bmatrix}. \tag{7}$$

Moreover, this matrix of the helical flagellum is as follows:

$$\begin{bmatrix} F_x^{\text{Thrust}} \\ F_y^{\text{Thrust}} \\ M_x^{\text{helix}} \\ M_y^{\text{helix}} \\ M_z^{\text{helix}} \end{bmatrix} = \overbrace{\begin{bmatrix} H_{xx}^{FU} & 0 & H_{xx}^{F\Omega} & 0 & 0 \\ 0 & H_{yy}^{FU} & 0 & H_{yy}^{F\Omega} & 0 \\ H_{xx}^{MU} & 0 & H_{xx}^{M\Omega} & 0 & 0 \\ 0 & H_{yy}^{MU} & 0 & H_{yy}^{M\Omega} & 0 \\ 0 & H_{zy}^{FU} & 0 & H_{zy}^{M\Omega} & H_{zz}^{M\Omega} \end{bmatrix}}^{G_{\text{helix}}} \begin{bmatrix} v_x \\ v_y \\ \Omega_x - \omega \cdot \cos\alpha \\ \Omega_y - \omega \cdot \sin\alpha \\ \Omega_z \end{bmatrix}, \tag{8}$$

$$[G_{\text{helix}}]_{5\times5} \begin{bmatrix} v_x \\ v_y \\ \Omega_x - \omega \cdot \cos\alpha \\ \Omega_y - \omega \cdot \sin\alpha \\ \Omega_z \end{bmatrix}_{5\times1} + [G_{\text{body}}]_{5\times5} \begin{bmatrix} v_x \\ v_y \\ \Omega_x \\ \Omega_y \\ \Omega_z \end{bmatrix}_{5\times1} = \begin{bmatrix} 0 \\ 0 \\ 0 \\ 0 \\ 0 \end{bmatrix}_{5\times1}. \tag{9}$$

Since the swimming robot is a free swimmer, the solution for forward velocity V and angular velocity Ω can be found by substituting the values of the hydrodynamic matrices of the body and helical flagellum, calculated in "Appendix A", in Eqs. (10–14). The results of the hydrodynamics model are extracted, as found in Eqs. (10–14):

$$v_x = \frac{H_{xx}^{F\Omega}(\omega \cdot \cos\alpha - \Omega_x)}{H_{xx}^{FU} + B_{xx}^{FU}}, \tag{10}$$

$$v_y = \frac{H_{yy}^{F\Omega}(\omega \cdot \sin\alpha - \Omega_y)}{H_{yy}^{FU} + B_{yy}^{FU}}, \tag{11}$$

$$\Omega_x = \omega \cdot \cos\alpha \cdot \frac{((H_{xx}^{MU} H_{xx}^{F\Omega}) - H_{xx}^{M\Omega}(H_{xx}^{FU} + B_{xx}^{FU}))}{((H_{xx}^{MU} H_{xx}^{F\Omega}) - (H_{xx}^{FU} + B_{xx}^{FU})(H_{xx}^{M\Omega} + B_{xx}^{M\Omega}))}, \tag{12}$$

$$\Omega_y = \omega \cdot \sin\alpha \cdot \frac{((H_{yy}^{MU} H_{yy}^{F\Omega}) - H_{yy}^{M\Omega}(H_{yy}^{FU} + B_{yy}^{FU}))}{((H_{yy}^{MU} H_{yy}^{F\Omega}) - (H_{yy}^{FU} + B_{yy}^{FU})(H_{yy}^{M\Omega} + B_{yy}^{M\Omega}))}, \tag{13}$$

$$\begin{aligned} \Omega_z &= \frac{PG_x}{B_{zz}^{M\Omega}} \left\{ H_{yy}^{FU} v_y - \frac{\omega \cdot \sin\alpha}{K} \right\} \\ K &= \frac{H_{yy}^{MU}}{(H_{yy}^{FU} + B_{yy}^{FU}) B_{yy}^{M\Omega}} - \frac{H_{yy}^{M\Omega}}{H_{yy}^{F\Omega} B_{yy}^{M\Omega}} - \frac{1}{H_{yy}^{F\Omega}}. \end{aligned} \tag{14}$$

According to the calculated kinematic variables, all of these variables include the functions of the geometrical parameters of the helical flagellum and swimmer body, inclination angle (α), spinning frequency, and the distance from the position of acting forces to the center of mass (PG_x). Parameter (PG_x) is dependent on the distribution of the mass in the body and helical flagellum and the position of acting forces.

According to Eqs. (10–14), when the helical flagellum axis is aligned with the body axis $(\alpha = 0^0)$, only v_x and Ω_x will remain, and the rest of the kinematic terms, including Ω_z, will be zero. In this case, the robot swims using forward velocity v_x and angular velocity Ω_x in a straight path along axis e_x.

Equations (10–14) are defined based on body coordinates. By defining (X, Y, Z) as inertia coordinates, the transformation of body coordinates to inertia coordinates can be done through Eq. (15):

$$\begin{bmatrix} V_x \\ V_y \\ V_z \end{bmatrix} = R_\varphi R_\theta R_\psi \begin{bmatrix} v_x \\ v_y \\ v_z \end{bmatrix}, \tag{15}$$

where R_{Trans} is defined as follows:

$$R_\varphi = 1, R_\theta = 1, R_\psi = \begin{bmatrix} \cos\psi & -\sin\psi & 0 \\ \sin\psi & \cos\psi & 0 \\ 0 & 0 & 1 \end{bmatrix}. \tag{16}$$

Using the kinematic variables in inertia coordinates, the control parameters for future closed-loop control can be investigated. The swimmer's turning velocity can be computed by velocity components $v_x$andv_y; further to that, using the angular velocity of the swimmer at axis$z$, the radius of curvature of the circular trajectory for the in-plane motion will be given as follows:

$$R = \frac{U}{|\Omega_z|} \quad , \quad U = (V_x^2 + V_y^2)^{1/2}. \tag{17}$$

3 Experimental test and model verifications

3.1 Experimental setup

In this study, an experimental prototype of a macro-scale swimmer robot inspired by the structure of prokaryote microorganism (the polar monotrichous bacterium: Vibrio) is used to validate the hydrodynamics model presented in Sect. 2.

This swimmer robot is composed of two main sections (body and helical flagellum), which are connected via a coupling. A view of this swimmer robot can be observed in Fig. 5.

Reynolds number can be expressed as a function of the relative object velocity with respect to the fluid velocity, U, the characteristic linear dimension L_{total} [in this paper, this characteristic is defined as overall length of swimmer robot (body length + helical tail)], the fluid density ρ, and the fluid dynamic viscosity μ as follows:

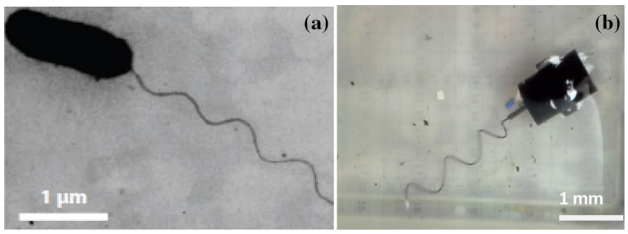

Fig. 5 **a** Microorganism with prokaryote propulsion (the polar monotrichous bacterium: Vibrio) (McCarter et al. 1988). **b** Fabricated biomimetic helical swimmer

$$Re = \frac{\rho U L}{\mu}. \tag{18}$$

To preserve the less-than-one Reynolds number conditions, the Buckingham PI theorem is employed and the liquid with high viscosity and the specific helical tail length were used. The fluid used in this experiment was silicone oil, with the kinematic viscosity of $10^{-3}\left(\frac{m^2}{s}\right)$ and density of $971\left(kg/m^3\right)$. The swimmer robot consists of two half bodies. There is enough space in each of these two casings for installing the needed equipment such as battery, motor, and connecting cables. Moreover, this design allows the equipment to be easily taken out when necessary (Fig. 6).

The propulsion system that drives this swimmer robot is composed of a rigid helical flagellum and dedicated DC motor. The motor actuates the helical flagellum and generates a thrust force by rotating in the counterclockwise direction along the body's major axis that enables the swimmer to move forward. The test was performed in a rectangular tank made of Plexiglas with dimensions of 300mm $\times$ 300mm $\times$ 700mm. The geometrical specifications of the swimmer and test equipment have been listed in Table 1.

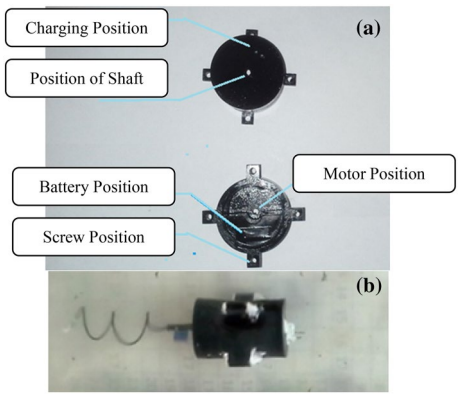

Fig. 6 **a** Two section of the swimmer body. **b** Submerged robot in the silicon oil tank

3.2 Investigation of the effects of inclination angles on the swimming robot's behavior

A helical swimming robot is designed, which has an inclination angle between the helical flagellum axis and its body axis. To determine and follow the swimmer's trajectory, a free channel was calibrated, and two Cannon cameras with the ability of capturing 100 frames per second were used. The distance between the swimmer and container walls at both ends is large enough to ignore the effects of the wall. Using the calibration method, the position of the swimmer at different times for each inclination angle was extracted. To investigate the effect of different inclination angles on the swimmer trajectory, the helical swimmer was characterized with three inclination angles. In the first test, for inclination angle of 10°, the swimming robot travels on a circular trajectory with a rough radius of 54.3 mm. The rotation of the swimmer at this inclination angle can be observed in Fig. 7.

To investigate the effect of increasing the inclination angle on the radius of swimmer's trajectory, the inclination angle between the helical flagellum and body axis increased. The experimental results demonstrate that the increase of the inclination angle reduces the radius of the circular trajectory, such that the radii of the trajectory decrease to 36.6 and 23.5 mm, respectively, at inclination angles of 15° and 25°. All the parameter values obtained for different inclination angles are listed in Table 2.

The experimental test shows how the swimmer with the inclination axis between the helical flagellum and body axis can swim on circular trajectories during swimming.

Table 1 Specification of the helical swimmer robot and the experimental setup

Parameters	Definition	Value	Unit
d_{body}	Cylindrical body diameter	28	mm
L_{body}	Cylindrical body length	42	mm
$2b$	Helical flagellum diameter	1	mm
$2h_{helix}$	Helical wave amplitude	11	mm
$L_{flagellum}$	Helical flagellum's length	32.5	mm
λ	Helical wave length	13	mm
β	Pitch angle	69.4	°
W	Total weight	28	g
ρ	Density of test fluid	971	kg/m^3
ν	Kinematic viscosity	0.001	
D_{motor}	Motor diameter	6	mm
L_{motor}	Motor length	18	mm
V_{motor}	Motor voltage	3	V
$vol_{battery}$	Battery volume	3.6*18*24	mm^3
$V_{battery}$	Battery voltage	3.7	V
–	CCD-Camera Specs	640-by-480 Pixels@100 fps	–

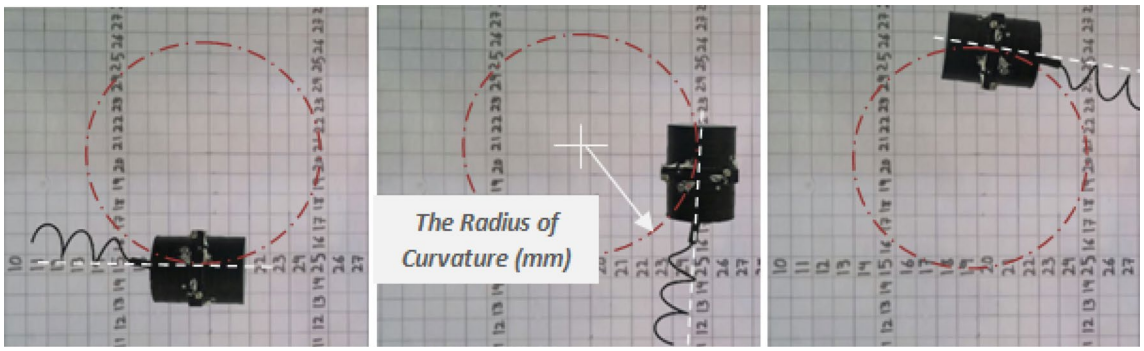

Fig. 7 The traveled trajectory for the helical swimmer robot with inclination angle α = 10, viewed from above the surface

Table 2 Experimental parameters obtained for different inclination angles

Deflection angle (°)	*R* radius of turning (mm)
10	54.3
15	36.6
25	23.5

3.3 Model verifications

Using the hydrodynamics modeling and the specifications of the fabricated swimming robot in Table 1, the behavior of the swimming robot is simulated at three different inclination angles $\alpha = 10°, 15°, 25°$. In this analysis, it is assumed that the helical tail rotates at the rotational frequency of 3 Hz, and there are no fitting parameters used in the simulated radius of curvature. In addition, as mentioned earlier, parameter (PG_x) depends on the distribution of the mass in the body and helical flagellum and the position of acting forces.

According to Eq. (19), by inclining the propulsion system at different inclination angles, the location of the mass center is almost less than 0.53 mm. Therefore, the center of the mass does not change significantly; by considering the fixed distribution of the mass in the body and the constant position for the acting forces and torques (Point P), it can be concluded that parameter (PG_x) is constant:

$$\begin{aligned} \mathrm{PG}_x &= \frac{L}{2} - L_{\mathrm{OG}} - L_{\mathrm{AP}} \\ &= 21 - (0.53 + 0.183\cos\alpha) - 3 \\ &= 17.47 - 0.183\cos\alpha, \end{aligned} \tag{19}$$

where $\mathrm{PG_x}$ denotes the distance from the positions of acting forces and torques to the mass center, $L_{\mathrm{AP}}$is the distance between the acting position and the end of body (here, $L_{\mathrm{AP}} = 3$ mm), and L_{OG} is the distance between the mass center and geometrical center of body ($L_{\mathrm{OG}} = \mathrm{LCG}$).

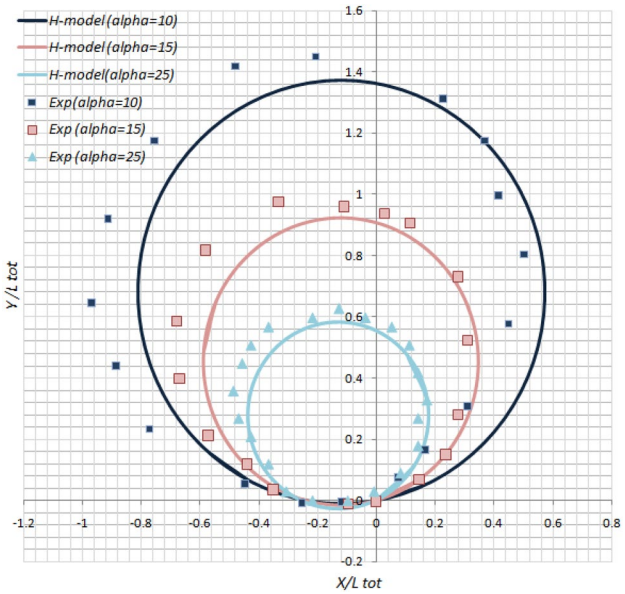

Fig. 8 Comparison of the results of experiment and simulation for the helical swimming robot at the three inclination angles, viewed from above the surface in the constant geometrical parameters

In Fig. 8, the results of experiment and simulation of the helical swimming robot at the three inclination angles are compared with each other. The hydrodynamics model predicts that the swimming robot's trajectory decreases by increasing the inclination angle in agreement with our experimental results. The smallest radius of curvature belongs to the inclination angle $\alpha = 25°$. The largest error for the radius of curvature can be seen at $\alpha = 10°$, where the most dominant parameter on this error is the wall effect. The differences between radius of curvature in the experiment and the simulation results for all tests can be defined as follows: $\frac{R_{\mathrm{exp}}}{R_{\mathrm{sim}}} = \mathrm{Dif}$. Accordingly, it can be concluded that, by increasing the inclination angle, the variation of this difference (Dif) value is small enough to ignore.

There are some differences in the results, for which the source of the errors can be discussed. Some of the assumptions used in this article caused the deviation between the results of the simulation and experiment. For instance, it is assumed that the walls are far enough, so that they will not significantly affect the behavior of the swimmer's motion; this assumption is probably effective in the experiment. Another assumption is to ignore all interactions between the swimmer's body and the helical tail. Another factor that contributes to the differences between the theory and experiment is the uncertainty in the experimental data and the uncertainty associated with the measurement equipment and the user.

4 Results of simulations

4.1 Simulations of traveled trajectories at different inclination angles

One of the important results of the hydrodynamics model is prediction of the trajectory that can be traveled by the swimming robot at different inclination angles. Depending on the various inclination angles from $0 \leq \alpha < 90$, the swimming robot swims on different trajectories. The traveled trajectories corresponding to each angle are simulated and depicted in Fig. 9. In all of these trajectories, the direction of rotation is counterclockwise because of positive angular velocity Ω_z on axis e_z, and the largest radius of curvature occurs at angle $\alpha = 0°$. At this angle, the swimming robot swims in a straight path. According to Fig. 9, the radius of curvature decreases by increasing inclination angle; however, in the range of $60 \leq \alpha \leq 80$, the variation of the radius of curvature is approximately constant, and the swimming robot rotates at the radius of curvature close to the body length ($R \leq L_{\text{body}}$). In this range of the inclination angle, only the position of the center of rotation changes, and the swimming robot rotates around its body. This behavior results from the linear relationship between the trajectory motion of the swimming robot and the inclination angle, as can be seen in Eqs. (10–14).

Furthermore, by switching ($\alpha \rightarrow -\alpha$), the direction of angular velocity ($\Omega_z \rightarrow -\Omega_z$) may change, causing the swimming robot to rotate in the clockwise direction. According to Fig. 10, at the inclination angle of $\alpha = 0°$, the swimming robot travels on a straight line with a constant forward velocity. When the inclination angle is larger than zero ($\alpha \neq 0°$), the swimming robot travels a whole circle with a specific radius of curvature.

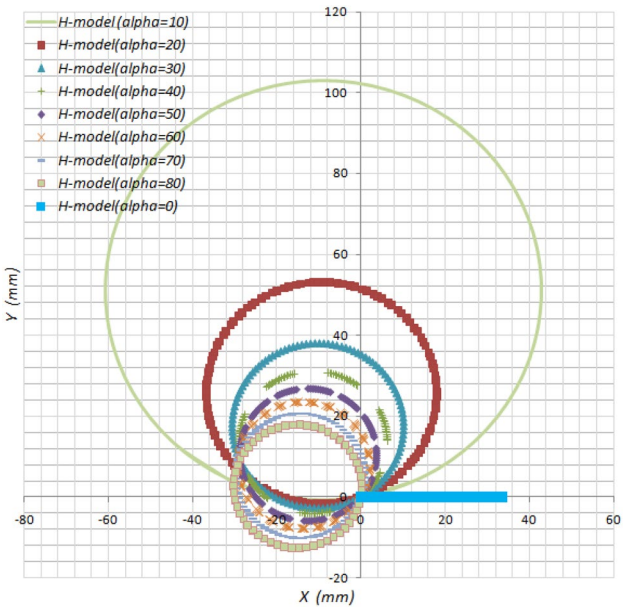

Fig. 9 Simulated trajectories for the helical swimmer robot with different inclination angle, viewed from above the surface

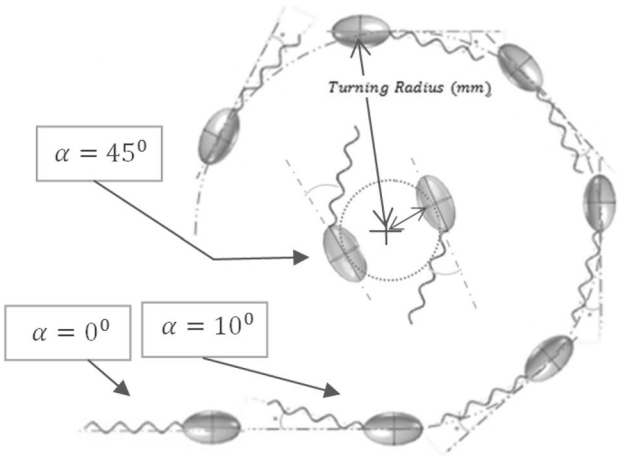

Fig. 10 Schematic simulated trajectories for the helical swimmer robot in the inclination angle ($\alpha = 0°$ and $\alpha = 10°$) and ($\alpha = 45°$) viewed from above the surface

4.2 Investigation of the effects of different inclination angles on radius of curvature and angular velocity

In this section, the effect of different inclination angles in the range of $0 < \alpha < 90$ on the radius of curvature and the angular velocity is investigated using the verified hydrodynamics model [according to Sect. (3.3)]. Figure 11a shows the variation of the radius of curvature at different inclination angles.

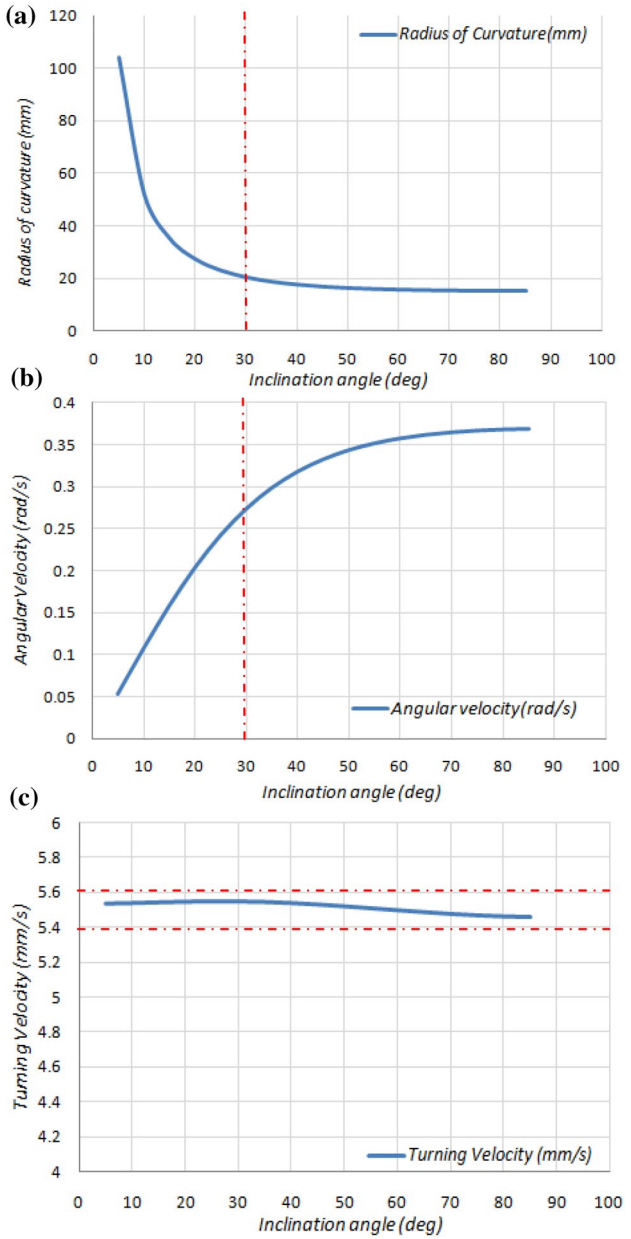

Fig. 11 **a** Variation of radius of curvature, **b** variation of angular velocity, and **c** turning velocity in different inclination angles

According to this figure, the radius of curvature decreases by increasing the inclination angle, and the highest variation belongs to the range of $0 < \alpha \leq 30$. However, in the range of $60 \leq \alpha \leq 80$, the variation of the radius of curvature is approximately constant, and the swimming robot rotates by the constant radius of curvature ($R \leq L_{\text{body}}$).

The results of the angular velocity in Z-direction or Yawing motion can be seen in Fig. 11b. The hydrodynamic parameters include a function of the rotational frequency of the helical flagellum, the geometrical parameters of body and tail, the distance between the positions of acting forces

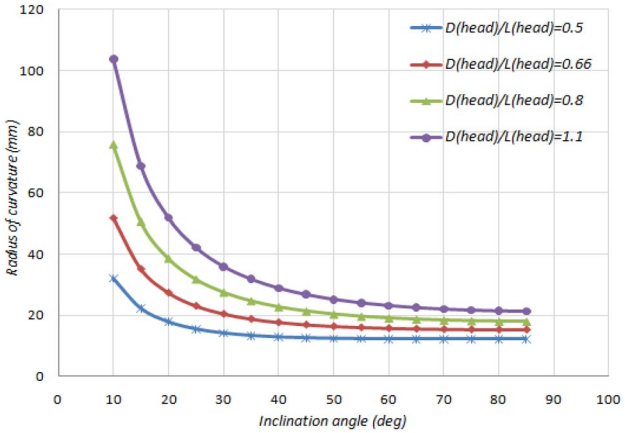

Fig. 12 Dependence of radius of curvature on the geometrical parameters of the swimmer body (d_{body}, L)

and torques from the center of mass of the helical swimming robot (PG_x), and the inclination angles. By considering the constant values of all parameters (the rotational frequency, the distance from the position of acting forces and torques to the center of mass (PG_x), and the geometrical parameters for body and tail), when the inclination angle increases in the range of $0 \leq \alpha < 90$, the angular velocity and turning torque will increase in Z-direction.

Consequently, the variations of the radius of the curvature and the angular velocity in the range of $30 < \alpha < 90$ are small enough to ignore, whereas the most effective range for variations in radius of curvature and the angular velocity is in the range of $0 < \alpha \leq 30$.

Figure 11c shows the variation of turning velocity at different inclination angles. According to this figure, the variation of turning velocity is in the range of $5.45 \leq U\left(\frac{\text{mm}}{\text{s}}\right) \leq 5.55$. Since the variation is very small, it can be concluded that the turning velocity has approximately constant values at different inclination angles, and it is a function of the rotational frequency and the geometrical parameters of the body and helical flagellum. Hence, it can be assumed that the swimming robot swims with a constant turning velocity at different inclination angles, considering the constant specification of the body and tail geometrical parameters at a constant rotational frequency.

4.3 Investigation of the effects of geometrical parameters on radius of curvature and turning velocity

According to Fig. 12, the effects of the geometrical parameters of the swimmer's body, such as diameter $\left(d_{\text{body}}\right)$ and length (L_{body}), are examined. In this research, it is considered that the distribution of the mass in the body is fixed;

therefore, the variation of the mass center is small enough that can be ignored. In addition, the position of acting force and torques (Point P) is fixed.

When the swimming robot has a thin body, it travels in a circle path with small radius of curvature while increasing the inclination angle. By increasing the diameter of the swimming body, the radius of curvature becomes larger than the thin shape, and the robot swims less quickly. Indeed, as the diameter of body increases, the drag force increases; then, the radius of the curvature increases, and the turning velocity of swimming robot decreases. Figure 13a–c show the effects of the normalized geometrical parameters of the helical flagellum, such as the wave amplitude$\left(\frac{h_{\text{helix}}}{L}\right)$, the radius of helix cross section $(\frac{b}{L})$, and the number of wavelength (n), on the radius of curvature and the turning velocity. In these figures, the dependence of the radius of curvature (R) on the three parameters is found to be decreasing as $\left(\frac{h_{\text{helix}}}{L}\right)$, $(\frac{b}{L})$, and (n) increase. The variations of the turning velocity in different geometrical parameters of the swimmer body and helical flagellum are listed in Table 3. The turning velocity decreases with $\left(\frac{d_{\text{body}}}{L_{\text{body}}}\right)$ and increases with increasing $\left(\frac{h_{\text{helix}}}{L}\right)$ and(n). According to this table, the variation of $(\frac{b}{L})$ is small enough to ignore in the simulation.

5 Conclusions

Many researchers have argued that helical propulsion is an appropriate and practical method for swimming in low-Reynolds number conditions. Although the linear propulsion characteristics of the helical swimmers have been studied extensively, the maneuverability characteristics of the swimming robot actuated by an internal actuation have not yet been elaborated clearly.

In this paper, a new method for maneuverability of the helical swimming robots with a single helical flagellum was introduced. A new method used here involves considering the inclination angle between the helical and body axes, so that the swimming robots can perform clockwise or counterclockwise turning maneuvers and move in a straight line. To investigate this new method and predict the swimmer's behavior at different inclination angles, the hydrodynamics model was presented based on the resistive force theory (RFT). Then, the swimmer's trajectories and hydrodynamic parameters, including its linear and angular velocities, at different inclination angles were extracted. Furthermore, an experimental prototype of a macro-size swimming robot with specific inclination angles was fabricated and tested to validate the presented hydrodynamics model. A comparison of obtained results indicated the good agreement between the theoretical and experimental results. The swimmer's behavior at different inclination angles was predicted using the validated hydrodynamics model. The results confirmed that the inclination angle caused the swimming robot to travel in the circular path; in addition, by increasing the inclination angle, the radius of curvature decreased. The highest variation was found in the range of $0 < \alpha \leq 30$; however, in the range of $60 \leq \alpha \leq 80$,

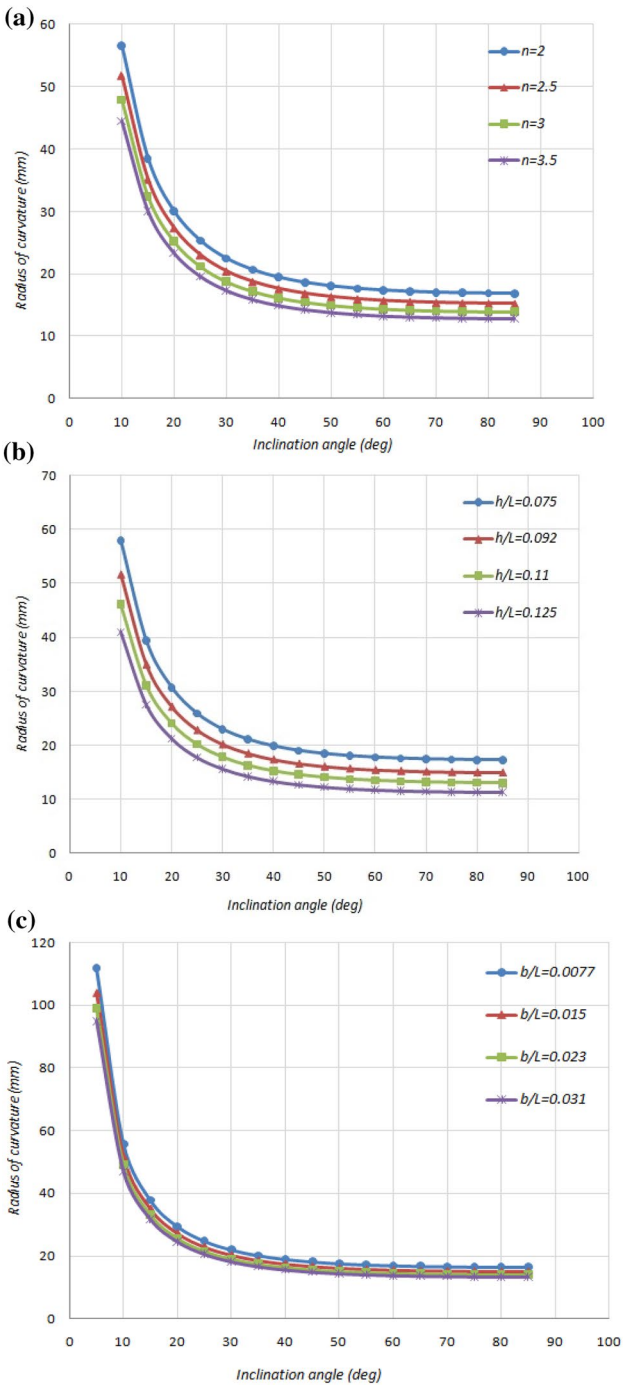

Fig. 13 Dependence of radius of curvature on the geometrical parameters of the helical flagellum

Table 3 Dependence of the results of turning velocity on the geometrical parameters of swimmer body and helical flagellum

Subject	Value			
$\frac{d_{\text{body}}}{L_{body}}$ (–)	0.5	0.66	0.8	1.1
Turning velocity (mm/s)	5.81	5.53	5.19	5.04
n (–)	2	2.5	3	3.5
Turning velocity (mm/s)	4.88	5.52	6.04	6.49
h/L (–)	0.075	0.092	0.11	0.125
Turning velocity (mm/s)	4.87	5.53	5.97	6.24
b/L (–)	0.0077	0.015	0.023	0.031
Turning velocity (mm/s)	5.47	5.53	5.51	5.42

the variation of the radius of curvature was approximately constant, and the swimming robot rotated at a constant radius of curvature ($R \leq L_{\text{body}}$). This maneuverability behavior resulted from the torque magnitude at different inclination angles, leading the swimming robot to undergo yaw motion; this torque increased by increasing inclination angle.

Finally, the hydrodynamics model illustrated that the turning velocity only depended on the rotational frequency and the geometrical parameters of the swimming robot; accordingly, by considering the constant values of the geometrical parameters, the turning velocity has constant value at different inclination angles. Using the extracted hydrodynamics model, the effect of geometrical parameters of body and helical flagellum was investigated on the radius of curvature and turning velocity. The results indicated that the radius of curvature increased and the turning velocity decreased due to the drag force exerted on the bluff body. In addition, by increasing the length and amplitude of the helical flagellum, the swimming robot traveled in circular paths with a smaller radius of curvature.

Therefore, for the swimming robot with a longer tail and a small-sized body, the turning velocity increased and the radius of curvature decreased.

The compared results indicated that this hydrodynamics model provided a viable alternative model for predicting the behavior of the helical swimming robot at various inclination angles in a range of design variables discussed here. In future works, a new mechanism with the ability to generate the inclination angle will be presented. In doing so, we will be able to control the parameters of this type of swimmers to accomplish predefined missions.

Appendix A

Hydrodynamics parameters

In this appendix, we present the value of the hydrodynamics parameters of the helical flagellum and body, which are represented by $H_{ij}^{\alpha\beta}$ and$B_{ij}^{\alpha\beta}$, respectively:

$$H_{xx}^{FU} = H_{yy}^{FU} = b_1, \quad H_{xx}^{F\Omega} = H_{yy}^{F\Omega} = b_2, \tag{18a}$$

$$B_{xx}^{FU} = a_{1x}, \quad B_{yy}^{FU} = a_{1y}, \tag{18b}$$

$$B_{xx}^{M\Omega} = B_{yy}^{M\Omega} = B_{zz}^{M\Omega} = a_2, \tag{18c}$$

$$H_{xx}^{MU} = H_{yy}^{MU} = c_1, \quad H_{xx}^{M\Omega} = H_{yy}^{M\Omega} = c_2\,, \tag{18d}$$

$$H_{zy}^{MU} = b_1 \cdot PG_x, \quad H_{zy}^{M\Omega} = b_2 \cdot PG_x\,, \tag{18e}$$

$$a_1 = \left(a_{1x}\sin^2\alpha + a_{1y}\cos^2\alpha\right), \tag{19a}$$

$$a_{1x} = \frac{16\pi\mu(L_{\text{body}}/2)e^3}{\left[\left(1+e^2\right)E - 2e\right]}\,, \quad a_{1y} = \frac{32\pi\mu(L_{\text{body}}/2)e^3}{\left[\left(3e^2-1\right)E + 2e\right]}, \tag{19b}$$

$$E = Ln\frac{1+e}{1-e}, \tag{19c}$$

$$e = \sqrt{(L_{\text{body}}/2)^2 - (D_{\text{body}}/2)^2}/(L_{\text{body}}/2), \tag{19d}$$

$$a_2 = \left((a_{2x} + (PG_x)^2 \cdot a_{1x})\sin^2\alpha \quad + \ (a_{2y} \cdot \cos^2\alpha)\right), \tag{19e}$$

$$a_{2x} = \frac{32\pi\mu(L_{\text{body}}/2)(D_{\text{body}}/2)^2e^3}{3\left[2e - \left(1-e^2\right)E\right]}, \tag{19f}$$

$$a_{2y} = \frac{32\pi\mu(L_{\text{body}}/2)(D_{\text{body}}/2)^2e^3\left(2-e^2\right)}{\left(3(e^2-1)\right)\left[\left(1+e^2\right)E - 2e\right]}\,, \tag{19g}$$

$$b_2 = h_{\text{helix}}n\lambda\,\left(\xi_n - \xi_t\right)\sin\beta, \tag{20a}$$

$$b_1 = n\lambda\,\cos\beta\left(\xi_n\tan^2\beta + \xi_t\right), \tag{20b}$$

$$c_1 = h_{\text{helix}}n\lambda\,\left(\xi_n - \xi_t\right)\sin\beta, \tag{20c}$$

$$c_2 = {h_{\text{helix}}}^2 n\lambda\,\cos\beta\left(\xi_t\tan^2\beta + \xi_n\right), \tag{20d}$$

$$m_{\text{tail}} = 4\mu\pi n\lambda d^2\cos\beta. \tag{20e}$$

References

Batchelor GK (1970), Slender-body theory for particles of arbitrary cross-section in Stokes flow. J Fluid Mech 44(3):419

Behkam B, Sitti M (2006) Design methodology for biomimetic propulsion of miniatur swimming robot. Trans ASME J Dyn Sys Meas Control 128:36–43

Berg H (2003) The rotary motor of bacterial flagella. Ann Rev Biochem 72:19–54

Brennen C, Winet H (1977) Fluid mechanics of propulsion by cilia and flagella. Annu Rev Fluid Mech 9:339–398

Chen B, Jiang S, Liu Y, Yang P, Chen S (2010) Research on the kinematic properties of a sperm-like swimming micro robot. J Bionic Eng 7:S123–S129

Chwang AT, Wu TY (1971) A note on the helical movement of microorganisms. Proc R Soc Lond B 178:327–346

Darnton NC, Turner L, Rojevsky S, Berg HC (2007) On torque and tumbling in swimming *Escherichia coli*. J Bacteriol 189:1756–1764

Edd J, Payen S, Stoller M, Rubinsky B, Sitti M (2003) Biomimetic propulsion mechanism for a swimming surgical micro-robot. In: Proc.IEEE/RSJ Int. Conf. Intell. Rob. Syst., Las Vegas, NV, USA, pp 2583–2588

Elgeti J, Winkler RG, Gompper G (2015) Physics of microswimmers-single particle motion and collective behavior: review. Rep Prog Phys 78:056601

Feng J, Cho SK (2014) Mini and micro propulsion for medical swimmers. Micromachines 5:97–113. https://doi.org/10.3390/mi5010097

Garcia J, Torre DL, Bloomfield VA (1977) Hydrodynamic theory of swimming of flagellated microorganism. Biophys J 20:49

Gray J, Hancock GJ (1955) The propulsion of sea-urchin spermatozoa. J Exp Biol 32:802

Ha N, Goo N, Yoon H (2011) Development of a propulsion system for a biomimetic thruster. Chinese Sci Bull 56:432–438

Johnson RE, Brokaw CJ (1979) Flagellar hydrodynamics a comparison between resistive force theory and Slender body theory. Biophys Soc 25:113–127

Keller J, Rubinow S (1976) Swimming of flagellated microorganisms. Biophys J 16:151

Lagua E (2016) Bacterial hydrodynamics. Annu Rev Fluid Mech 48:105–130

Lighthill J, Lighthill M (1975) Mathematical biofluid dynamics. Society for Industrial and Applied Mathematics, Philadelphia

Liou W, Yang Y (2015) Numerical study of low-Reynolds number flow over rotating rigid helix: an investigation of the unsteady hydrodynamic force. Fluid Dyn Res 47:045506 (**IOP publication**)

McCarter L, Hilmen M, Silverman M (1988) Flagellar dynamometer controls swarmer cell differentiation of V. parahaemolyticus. Cell 54:345–351

Nelson BJ, Kaliakatsos I, Abbott JJ (2010) Micro robots for minimally invasive medicine. Annu Rev Biomed Eng 12:55–85

Nourmohammadi H, Keighobadi J, Bahrami M (2016) Design, dynamic modelling and control of a bio-inspired helical swimming microrobot with three-dimensional manoeuvring. Trans Inst Meas Control (SAGE) 39(Issue 7):1036–1046

Pak Sh, Lauga E (2014) Theoretical models in low-Reynolds-number locomotion. In: Duprat C, Stone HA (eds) Low-Reynolds-number flows: fluid-structure interactions. Soft Matter Series. Royal Society of Chemistry

Peyer KE, Mahoney AW, Zhang LJ, Abbott BJ, Nelson (2012) Bacteria-inspired microrobots. Microbiorobotics. https://doi.org/10.1016/B978-1-4557-7891-1.00007-4 (**Elsevier Inc**)

Purcell EM (1997) The efficiency of propulsion by a rotating flagellum. Natl Acad Sci USA (PNAS) 94:11307–11311

Reynolds O (1883) An experimental investigation of the circumstances which determine whether the motion of water shall be direct or sinuous and of the law of resistance in parallel channels. Philosoph Trans R Soc Lond 174:935–982

Sitti M (2007) Microscale and nanoscale robotics systems [grand challenges of robotics. IEEE Robot Autom Mag 14(1):53–60

Tabak AF, Yesilyurt S (2013) Improved Kinematic models for two-link helical micro/nano-swimmers. IEEE Transact Robot 30:14–25

Taute KM, Gude S, Tans SJ, Shimizu TS (2015) High-throughput 3D tracking of bacteria on a standard phase contrast microscope. Nature Commun 6:8776

Temel FZ, Yesilyurt S (2013) Simulation-based analysis microrobots swimming at the center and near the wall of circular minichannels. Microfluid Nanofluid 14(1–2):287–298

Tottori S, Zhang L, Qiu F, Krawczyk K, Obregón Al, Nelson BJ (2012) Magnetic helical micromachines: fabrication, controlled swimming, and cargo transport. Adv Mater 24:811–816

Xie L, Altindal T, Chattopadhyay S, Wu X (2011) Bacterial flagellum as a propeller and as a rudder for efficient chemo taxis. PNAS 108(6):2246–2251

Xu T, Hwang G, Andreff N, R´egnier S (2015) Influence of geometry on swimming performance of helical Swimmers using DoE, Springer. J Microbiorobotic 31(1):117–127

Ye Z, R´egnier St, Sitti M (2013) Rotating magnetic miniature swimming robots with multiple flexible flagella. IEEE Trans Rovotics. http://www.rowland.harvard.edu/labs/bacteria/movies/showmovie.php?mov=fluo_curly1[22]

Zhang L, Peyer K, Nelson BJ (2010) Artificial bacterial flagella for micromanipulation. Lab Chip 10(17):2203–2215